

Interlocking friction governs the mechanical fracture of bilayer MoS₂

Gang Seob Jung^{1*}, Shanshan Wang^{2*}, Zhao Qin¹, Francisco J. Martin-Martinez¹, Jamie H. Warner^{2†}, and Markus J. Buehler^{1,3†}

¹ Laboratory for Atomistic and Molecular Mechanics (LAMM), Department of Civil and Environmental Engineering, Massachusetts Institute of Technology, 77 Massachusetts Ave., Cambridge 02139, MA, USA

²Department of Materials, University of Oxford, Parks Road, Oxford, OX1 3PH, United Kingdom

³Center for Computational Engineering, Massachusetts Institute of Technology, 77 Massachusetts Ave., Cambridge, MA 02139, USA

†Email: (jamie.warner@materials.ox.ac.uk) or (mbuehler@mit.edu).

*These authors contributed equally to this work

Abstract: Molybdenum disulfide (MoS₂) monolayer is a two-dimensional (2D) material, which is expected to provide the next generation of electronic devices together with graphene and other nanomaterials. Due to its significance for future electronics applications, gaining a deep insight of the fundamental mechanisms upon MoS₂ fracture is crucial to prevent mechanical failure towards reliable applications. Here, we report direct experimental observation and atomistic modeling of the complex failure behaviors of bilayer MoS₂, revealing highly variant interlayer frictions, elucidated with *in-situ* transmission electron microscopy and large-scale reactive molecular dynamics simulations. Our results provide systematic understanding of the effects that different stacking and loading conditions cause on the failure mechanisms and crack-tip behaviors in bilayer MoS₂ systems. Our findings unveil essential properties in fracture of this 2D material and provide mechanistic insight into its mechanical failure.

Keywords: MoS₂, van der Waals bilayer, crack propagation, two-dimensional material, *in-situ* TEM

Submitted to: *ACS Nano*

Fundamental fracture mechanics is of crucial concern for materials engineering and subsequent applications, which requires understanding the underlying mechanisms governing crack propagation in broad range of scientific disciplines.¹⁻³ As a post-graphene material, molybdenum disulfide (MoS₂) monolayer is a two-dimensional (2D) material from the transition metal dichalcogenide (TMD) family that has attracted considerable attention due to its remarkable electronic and optoelectronic properties.⁴⁻⁷ These 2D materials show distinct mechanical behaviors⁸ and their atomically thin structures provide opportunities for observing atom dynamics⁹⁻¹⁰ and manipulating atomic configurations.¹¹ Differently from bulk materials, a single bond breaking in these 2D structures can result in crack propagation due to its atomic thinness. Therefore, the behavior of crack-tip in 2D materials is strongly affected by atomic scale features near the crack-tip, *e.g.*, defects and grain boundaries.¹²⁻¹³

Furthermore, there are emerging applications and fundamental engineering arising from the addition of more layers to the system, *e.g.*, electro-mechanics¹⁴⁻¹⁶ and van der Waals (vdW) heterostructures,¹⁷⁻¹⁹ where the interlayer interaction becomes more crucial for their fracture.

Thus, characterizing interlayer interactions and understanding their roles in the mechanical stability and failure are of great importance for the development of devices based on the combination of 2D materials. To understand the multilayer 2D systems, the stacking geometries and binding energies of differently stacked bilayer MoS₂ systems have been reported.²⁰⁻²¹ Despite these previous initiatives, the atomic-scale mechanics of crack-tip behaviors in multilayer MoS₂ systems have been elusive so far due to challenges associated to its direct experimental observation and development of predictive atomic-scale models. Specifically, it is quite elusive how the interlayer interaction of MoS₂ may interplay with the crack-tip behaviors in one of the layers.

Our previous study has demonstrated that *in-situ* aberration-corrected transmission electron microscopy (AC-TEM) and molecular dynamics (MD) simulations are efficient tools to investigate the dynamics of crack-tip behaviors and fracture of MoS₂ monolayer.¹² By utilizing these tools, we report here the dynamics of crack propagation in suspended bilayer MoS₂ and address questions related to the effects of the uncracked layer on crack propagation in the cracked layer. Our finding reveals atomic-scale features and interlayer interactions of the multilayer system with 2D materials, which impacts the bottom-up design of vdW heterostructures and applications of electro-mechanics.

RESULTS AND DISCUSSION

One of the most promising methods to produce high-quality and large-area MoS₂ is chemical vapor deposition (CVD). By adjusting the synthesis parameters properly, the MoS₂ samples contain regions of both monolayer and bilayer. In our experimental setup, cracks are introduced into MoS₂ by popping a strained MoS₂ membrane with a focused high-energy electron beam (Figure 1a, See Methods) to cause fractures that enable the observation of the crack-tip behaviors with AC-TEM. The cracks that initially appear in monolayer regions then propagate into bilayer domains in Figure 1b (i-iv). The single atom resolution of AC-TEM and the application of Fast Fourier Transformation (FFT) to TEM images (See Methods), enables the extraction of specific lattice information in the reciprocal space to successfully reconstruct the atomic details of each layer in the bilayer MoS₂ as demonstrated in Figure 1b(v-viii).

To obtain a reliable forcefield for performing MD simulations that are able to reproduce the behavior of crack-tips in bilayer MoS₂ system, we adapted the reactive forcefield (REBO) parameters by using dispersion-corrected DFT (Density Functional Theory) calculations to describe well both mechanical properties of intralayer and interlayer interactions of MoS₂ (See SI Methods 1-3). As shown in Figure 1c, the crack behavior with bilayer region is well captured in Figure 1c. Then, the subsequent MD simulations, allow us to systematically measure the friction between two layers with different stacks and loading directions by using a circular top layer. This is shown in Figure 2a (See SI Method 4). The magnitude of the friction significantly depends on the stacking and loading conditions (Figure 2b). The results show that frictions in \pm armchair (AC) directions with 2H and 3R stacks can reach 10 times higher than turbostratically-stacked bilayer systems. The origin of difference for 2H and 3R with respect to turbostratically-stacked systems are expected to come from different binding energies as shown in Table S1 and S2. However, the binding energies of 2H or 3R stacking are only ~ 1.5 times larger than those of AA stacking. Instead, analyzing the relative position of sulfur atoms in top and bottom layers indicate geometric effects on the friction. As shown in Figure 2c, sulfur positions in \pm zigzag (ZZ) directions are highly symmetric while sulfur positions in \pm AC directions are asymmetric. In fact, the peaks of friction forces occur when

the sulfur atoms of the top layer align to the sulfur atoms of the bottom layer. Our results show that the slopes are equal to all peaks due to the geometry and number of interacting sulfur atoms per unit length. Therefore, we conclude that such large difference result not from the vdW interaction itself but geometrical interlocking between two layers.

Also, we found that the friction per unit area of stacked bilayer is likely to decrease as the stacked areas increase (See [Tables S4 - S8](#)) because local ripples facilitate the sliding as the stacked areas increase. Also, we have evaluated the loading rate dependence. The results show that the friction values are likely to decrease as the loading rate decrease as shown in [Figure S3](#). However, the friction values of 2H and 3R systems are less sensitive to the loading rate compared to turbostratically-stacked layers, which means that the friction from well-stacked layers can be much stronger than the friction coming from turbostratically-stacked layers at the slow loading rate limit. These unique geometrically interlocking friction mechanisms of MoS₂ allow us to understand complicated crack-tip behaviors observed with *in-situ* AC-TEM.

Crack tips in turbostratically-stacked bilayer MoS₂ region: crack blocking

[Figure 3](#) shows the experimental observation of crack propagation in turbostratically-stacked bilayer regions with AC-TEM, together with MD results. In turbostratically-stacked systems one of the layers can be removed in AC-TEM images by using a mask in Fourier space to study the crack in detail without the interference of the second layer. The AC-TEM images reconstructed by these means show the atomic structures of both the cracked and uncracked regions separately, which can be directly compared to the simulations results. Both AC-TEM images and MD indicate that the crack prefers the zigzag direction for propagating, and as a consequence the sliding of the cracked layer with respect to the uncracked one generate different moiré pattern in [Figure 3a and d](#).

To see how the friction from the different stacking can disturb the crack propagation, we also performed MD simulations with various angles of stacked conditions (See [Crack blocking in Methods](#) and [Figure S3a](#)). Due to the elastic energy, a crack naturally propagates into the circular bilayer regions. The propagation of the crack is disturbed drastically and finally stops at the center of circular region with 0° (3R) and 60° (2H). However, other stacking angles (*e.g.*, 15°, 30°, and 45°) cannot disturb cracks enough as shown in [Figure S3b](#) (See [Supporting movies 1 and 2](#) for 15° and 2H). Additionally, [Figure 3](#) shows the good agreement between the moiré patterns that appear during the crack propagation with 15° rotated turbostratic stack from experimental observation and MD simulations. The asymmetric moiré patterns along the crack result from asymmetric friction from the other layer.

Crack propagation through the entire bilayer region: coherent fracture

[Figure 4](#) shows two distinct fracture behaviors in suspended 2H-stacked MoS₂ that are generated by puncturing the membrane with the electron beam irradiation in a monolayer region. The crack on the left propagated too fast to be captured with the AC-TEM imaging technique, while the crack on the right propagated slowly enough to be tracked. Despite the fast propagation of the first crack, the image shows a complete fracturing of both layers, while the slow crack is confined in one layer without any interruption of the second layer. Although friction force from fast crack propagation should be higher than that from slow propagation, this loading rate dependence is not sufficient to explain the coherent fracture.

To test whether the uncracked layer breaks due to the crack propagation in the second layer, we performed MD simulations of a 30 x 40 nm rectangular shape bottom layer with an 8 nm length initial crack. To evaluate the differences coming from stacking conditions, 30x30 nm

square-shaped top layer is stacked with 0° (3R), 60° (2H), and 15° . The top layer is assumed to be semi-infinite with periodic boundary conditions (See [Coherent fracture in Methods](#) and [Figure 7a](#)). We found that the top layer does not break even if the pre-strain increases in both layers, which corresponds to faster propagation due to higher elastic energy.

The crack propagations cause local ripples in the cracked layer and it disturbed the coherent behaviors (consisting 2H stack) as shown in [Figure 4e](#), reducing the friction significantly. Once the 2H stacking is distorted, it does not recover its alignment due to the mismatching strains at both layers. However, this behavior changes drastically if the top layer has a small flaw on the crack propagation path. Due to this flaw, the regions near the flaw are not well stacked in 2H arrangement anymore before the crack path, allowing coherent movement cause effective tensile stress near the crack tip after first crack passed as shown in [Figure 4f](#). Therefore, the small flaw becomes a crack-tip following the first crack path. It is important to note that this flaw is too small to break along itself. Also, the coherent fracture happens with 3R, but not with turbostratic stacks with the same conditions, as shown in [Figure S6b](#) (See [Supporting movies 3 and 4](#) for 15° and 2H stacks with a 2nm flaw).

Cracks in 2H stacked bilayer MoS₂: crack branching

[Figure 5a](#) shows a region in the bilayer MoS₂ where the 1st crack tip is in the monolayer region and the 2nd crack goes through both layers. There is lattice distortion along the 1st crack path, which could be a result from defects and grain boundaries. As shown in the [Figure 5e](#), moiré patterns are observed at the front of the 1st crack. Although these irregular moiré patterns could be thought to arise from a local ripple of one layer, the remaining tensile strain of the other layer prevents the local ripple to appear with such extremely confined width and non-straight shape²². Also, if this comes from grain boundaries, good 2H-stacking alignment in other regions is not well explained. Thus, it is reasonable to conclude that the distortion comes from defects. These unique structures can happen when two 2H-stacked separated triangles on monolayer MoS₂ combine during CVD growth-process. Furthermore, the 1st crack path is on the defected region of the 2nd layer, which can result from weakening friction in the non-coherent 2H-stacked regions. Surprisingly, the 1st crack branches into highly complicated paths ([Figure S8](#)), in contrast to other observed cracks.

To understand this complex crack-tip behavior in the system, we simplified the model with some critical features. First, the entire system is considered as a 2H-stacked bilayer MoS₂. Second, A thin defected region is prepared in the uncracked 2nd layer. Finally, the system is constrained not only in the direction perpendicular to the crack propagation but also in the crack propagation direction, which implies fixing all boundaries. Within these settings, we simulated a 40x40 nm bilayer system with an initial crack inserted in the 1st layer. The 2nd layer has 2nm-width defect regions with different defect ratios, as shown in [Figure S7a](#) (See [Crack branching in Methods](#)). As the defect ratio increases, the crack path becomes more disturbed and eventually branches when 10% defects ratio is reached ([Figure S7](#) and [Figure 5i](#) and [Supporting movies 5 and 6](#) for 0% and 10%).

Branched directions of the crack also show the same trend with AC-TEM images. One crack is likely to pass straight following a zigzag edge direction, and the other crack is deflected to the armchair edge direction. The asymmetry in the friction forces due to non 2H-stacking controls branched directions shown in [Figure 5i](#). The branching points in AC-TEM images show non 2H-stacked moiré patterns, as well as the same branching directions from MD simulations. While one crack propagates straight, the other one deflects, as shown in [Figure 5 and Figure S8](#). In AC-TEM images, the branched cracks run parallel and leave islands behind as shown in [Figure S8](#), which is not mechanically driven without sliding but induced by

electron beams because the islands become smaller by losing atoms without moiré pattern changes.

CONCLUSION

We report that bilayer MoS₂ has unique interlayer friction between the layers that depend not only on the stacking conditions but also on the loading conditions. Especially, 2H and 3R stacking arrangements show extremely high static friction compared to turbostratically-stacked bilayers due to their geometrical interlocking coming from sulfur-to-sulfur positions. This is the first report of the geometrical interlocking mechanism in bilayer MoS₂. Also, we observed various crack-tip behaviors in bilayer MoS₂ system: 1) a crack can either propagate or be blocked due to the different frictions. 2) a crack in the first layer can induce breaking of the other layer. 3) a crack in the first layer branches due the existence of defects or atomic configuration in the other layer. The observed complex behaviors can be explained by the principles we derived:

- High friction from sulfur-to-sulfur interlocking of 2H and 3R stacks
- Low friction of turbostratic stacks
- Loading-directional dependence of slip-stick frictions

These essential insights into complex fracture of bilayer MoS₂, can also apply to other transition metal dichalcogenide (TMD) materials, which further increases the relevance of this scientific contribution.

METHODS

CVD synthesis and transfer of MoS₂ sample

MoS₂ monolayers and bilayers were prepared using a similar approach to that previously reported.²³ Molybdenum trioxide (MoO₃, ≥99.5%, Sigma-Aldrich) and sulphur (S, ≥99.5%, Sigma-Aldrich) powder were used to grow monolayer MoS₂ on a SiO₂/Si substrate (300 nm thick SiO₂) by chemical vapor deposition (CVD) at atmospheric pressure. Two furnaces were used to enable temperature control on both the precursors and the substrate. The heating temperatures for S, MoO₃ and SiO₂/Si substrate were ~ 180, ~300, and ~800 °C, respectively, with argon used as the carrier gas. To avoid cross-contamination between MoO₃ and S, MoO₃ powder was placed in an inner tube having a smaller diameter, which was then inserted into the larger one-inch quartz tube. The S powder was loaded in the outer quartz tube. The substrate was oriented vertically to increase the uniform growth area of MoS₂ film. This CVD method grew continuous monolayer MoS₂ films with ~10% of the area covered by bilayers. The as-grown product was checked under the optical microscope and the regions having a high percentage of bilayer MoS₂ were marked for the following transfer procedure. MoS₂ was transferred onto the Si₃N₄ TEM grid (Agar Scientific AG21580) *via* a standard polymer-based method. The surface of the MoS₂/SiO₂/Si substrate was first spin-coated with a thin film of poly (methyl methacrylate) (PMMA) followed by floating it on a 1 M potassium hydroxide (KOH) solution to etch the SiO₂ away. After the PMMA/MoS₂ film was detached from the Si substrate, the film was rinsed in deionized water for several times. Subsequently, the regions in the film with a high percentage of bilayer MoS₂ were scooped up using a holey Si₃N₄ grid. The grid was dried overnight in air followed by baking at 180 °C for 15 minutes. Finally, the grid was submerged in acetone for 8 hours to remove PMMA.

Transmission electron microscopy and TEM data processing

High-resolution TEM imaging was conducted using Oxford's JEOL JEM-2200MCO field emission gun transmission electron microscope with a CEOS imaging aberration corrector under an accelerating voltage of 80 kV. AC-TEM images were recorded using a Gatan Ultrascan $4k \times 4k$ CCD camera (frame speed: ~ 25 fps) with 1-2 s acquisition time. We took one frame approximately every 10-20s in our AC-TEM imaging depending on the speed of the crack propagation and the imaging condition adjustment. Images were processed using the software of ImageJ. They were initially adjusted with a band-pass filter (between 100 and 1 pixel) to modify the long-range non-uniformity on the illumination intensity, and then smoothed by applying a Gaussian blur (2 pixels). For turbostratically assembled bilayer MoS₂ with a twist angle except integral multiple of 60° , the lattice configuration corresponding to each layer can be separately reconstructed. It was realized by first doing the FFT of the AC-TEM image followed by applying a mask to the 2D FFT image to only choose reflexes contributed by one layer of the bilayer MoS₂ in the reciprocal space. Finally, do the inverse FFT to reconstruct the lattice structure of this layer in the real space. Cracks were generated by illuminating suspended MoS₂ to the focused electron beam under 80 kV, which is similar to prior work¹². The crack emanated from either a bilayer region or a monolayer area, which can subsequently move into bilayer domains. The generation of the fast fracture in MoS₂ by a focused electron beam at the initial stage was due to a homogeneous in-plane tension in suspended MoS₂ introduced by the baking process during transfer, which is similar as popping a tight drumhead by a sharp needle. The crack continuously propagated by a proper dose of the electron beam irradiation on MoS₂ during imaging, as the electron beam produced a tiny force at the crack tip due to the formation of line defects along fractured edges and the curling up of the freshly cracked edges.

Molecular dynamics simulations

Molecular dynamics simulations in this study were performed via LAMMPS package.²⁴ Reactive Empirical Bond Order (REBO) forcefield (FF)²⁵⁻²⁷ is utilized for the interatomic potential. We obtained the binding energy as a function of distance between two layer from our DFT calculations with DFT-D2 correction,²⁸ and utilized the data to optimize the previous parameters.^{12, 29} The obtained binding energy and equilibrium distances for 2H (AA'), 3R(AB), and AA stacks show good agreement with previous DFT studies.^{21, 30} We tuned REBO parameters for both the interatomic interaction and vdW interaction, which successfully described monolayer stress-strain curves, elastic constants, and bilayer interactions from DFT calculations (See **SI Methods**). Based on this optimized FF, we performed simulations to measure the friction forces between two layers with different stack conditions, loading directions, and loading rates. We utilized Steered Molecular Dynamics (SMD)³¹ to pull the top layer in the zigzag and armchair directions, allowing natural deformation and localized sliding under various loadings, where the method is generally utilized for deformation of complex biomaterials³² (See **SI Methods** for more details).

Crack blocking: Crack propagation into stacked finite bilayer regions

We prepared a 30x50nm rectangular MoS₂ layer (bottom layer) for the crack region with a circular layer (top layer) with a 14nm radius for the uncracked region as shown in **Figure S4a**. The circular regions are stacked in six different ways: 0° (3R), 15° , 30° , 45° , and 60° (2H) rotated. In the beginning, the systems are stretched with 3.2% tensile strain in the x direction, which allows crack propagation and breaks entire layer without the circular layer as shown in **Figure S4b**. After energy minimization, the system is relaxed with NVT ensemble at low temperature 10K for 100ps with 1fs time step. We note that the bottom layer is still pre-

stretched but the top layer is fully relaxed without rotation. Then, NVE ensemble is applied to ignore the undesired effects from thermostat before a crack inserted in the bottom layer. This process helps us to correctly capture the subtle differences from different stacks. After a sharp crack ($l_c = 15\text{nm}$) is inserted in the bottom layer and the crack propagation is observed as shown in [Figure S4b](#).

Coherent fracture: Crack propagation into stacked semi-infinite bilayer regions

Instead of finite circular layer, a semi-infinite top layer that is large enough to be pre-stretched with the bottom layer is modeled. A square layer ($30 \times 30 \text{ nm}$) is stacked on the bottom layer with different angles: 0° (3R), 15° , and 60° (2H). The bottom layer is $30 \times 40\text{nm}$ and the major crack length ($l_c = 8\text{nm}$) in the bottom layer is set to 8nm . Different flaws are introduced in the top layer from 0 to 3nm crack (l_{c2}) on the crack-path in the bottom layer as shown in [Figure S6a](#). The flaw lengths are too short to allow the crack propagation in the top layer with the applied pre-strain ($\sim 5\%$).

Crack branching: Cracks in 2H stacked bilayer MoS₂

From the experimental observation in [Figure 5](#), we prepared the $40 \times 40\text{nm}$ square layer for the top and bottom layer with 2H-stack as shown in [Figure S7a](#). First, different ratios of defects are introduced in the defect region of top layer where the width is 2nm and the length is 40nm . Each model is relaxed with 4% pre-strain in the x direction. After energy minimization, the system is relaxed with NVT ensemble at 10K for 100ps . The ensemble is changed from NVT to NVE and a crack ($l_c \sim 8\text{nm}$) is introduced in the bottom layer. The stored strain energy allows the crack start to propagate, and the natural behaviors of both layers are observed. The left and right boundaries are fixed in the x direction and top and bottom boundaries are fixed in the y direction with non-periodic boundary condition, mimicking the main features from the experimental structure in [Figure 5](#).

Supporting Information

SI Methods

1. DFT calculation for binding energy of MoS₂ bilayer
2. Parameter optimization for vdW binding energy (Reactive FF, REBO)
3. Parameter optimization for mechanical properties of monolayer MoS₂ (Reactive FF, REBO)

4. Interlocking friction force: MD simulations

Supporting Tables 1: DFT calculations for binding energy

Supporting Tables 2: DFT calculations for geometry

Supporting Tables 3: Tuned LJ parameters of current forcefield

Supporting Tables 4: Geometric parameters and elastic constants

Supporting Tables 5-8: The values of interlayer frictions

Supporting Figures 1-8

Supporting Movies 1-6

ACKNOWLEDGEMENTS

Funding and resources: The authors GS.J, Z.Q., F.J M-M and M.J.B acknowledge support by the Office of Naval Research (Grant No. N00014-16-1-233) and DOD-MURI (Grant No. FA9550-15-1-0514). We acknowledge support for supercomputing resources from the Supercomputing Center/KISTI (KSC-2017-C2-0013).

Author contributions: All the authors contributed to the current work and writing the paper.

Competing interests: The authors declare that they have no competing interests. Data and materials availability: All data needed to evaluate the conclusions in the paper are present in the paper and/or the Supporting Information. Additional data related to this paper may be requested from the authors.

REFERENCES

- (1) Buehler, M. J.; Gao, H., Dynamical fracture instabilities due to local hyperelasticity at crack tips. *Nature* **2006**, *439* (7074), 307-310.
- (2) Kermode, J. R.; Albaret, T.; Sherman, D.; Bernstein, N.; Gumbsch, P.; Payne, M. C.; Csanyi, G.; De Vita, A., Low-speed fracture instabilities in a brittle crystal. *Nature* **2008**, *455* (7217), 1224-1227.
- (3) Livne, A.; Bouchbinder, E.; Svetlizky, I.; Fineberg, J., The Near-Tip Fields of Fast Cracks. *Science* **2010**, *327* (5971), 1359.
- (4) Wang, Q. H.; Kalantar-Zadeh, K.; Kis, A.; Coleman, J. N.; Strano, M. S., Electronics and optoelectronics of two-dimensional transition metal dichalcogenides. *Nat Nano* **2012**, *7* (11), 699-712.
- (5) Jariwala, D.; Sangwan, V. K.; Lauhon, L. J.; Marks, T. J.; Hersam, M. C., Emerging Device Applications for Semiconducting Two-Dimensional Transition Metal Dichalcogenides. *ACS Nano* **2014**, *8* (2), 1102-1120.
- (6) RadisavljevicB; RadenovicA; BrivioI; GiacomettiV; KisA, Single-layer MoS₂ transistors. *Nat Nano* **2011**, *6* (3), 147-150.
- (7) Splendiani, A.; Sun, L.; Zhang, Y.; Li, T.; Kim, J.; Chim, C.-Y.; Galli, G.; Wang, F., Emerging Photoluminescence in Monolayer MoS₂. *Nano Lett.* **2010**, *10* (4), 1271-1275.
- (8) Lee, C.; Li, Q.; Kalb, W.; Liu, X.-Z.; Berger, H.; Carpick, R. W.; Hone, J., Frictional Characteristics of Atomically Thin Sheets. *Science* **2010**, *328* (5974), 76.
- (9) Warner, J. H.; Rummeli, M. H.; Ge, L.; Gemming, T.; Montanari, B.; Harrison, N. M.; Büchner, B.; Briggs, G. A. D., Structural transformations in graphene studied with high spatial and temporal resolution. **2009**, *4*, 500.
- (10) Warner, J. H.; Margine, E. R.; Mukai, M.; Robertson, A. W.; Giustino, F.; Kirkland, A. I., Dislocation-Driven Deformations in Graphene. *Science* **2012**, *337* (6091), 209.
- (11) Robertson, A. W.; Allen, C. S.; Wu, Y. A.; He, K.; Olivier, J.; Neethling, J.; Kirkland, A. I.; Warner, J. H., Spatial control of defect creation in graphene at the nanoscale. **2012**, *3*, 1144.
- (12) Wang, S.; Qin, Z.; Jung, G. S.; Martin-Martinez, F. J.; Zhang, K.; Buehler, M. J.; Warner, J. H., Atomically Sharp Crack Tips in Monolayer MoS₂ and Their Enhanced Toughness by Vacancy Defects. *ACS Nano* **2016**, *10* (11), 9831-9839.
- (13) Jung, G. S.; Qin, Z.; Buehler, M. J., Molecular mechanics of polycrystalline graphene with enhanced fracture toughness. *Extreme Mechanics Letters* **2015**, *2* (0), 52-59.
- (14) He, K.; Poole, C.; Mak, K. F.; Shan, J., Experimental Demonstration of Continuous Electronic Structure Tuning via Strain in Atomically Thin MoS₂. *Nano Lett.* **2013**, *13* (6), 2931-2936.
- (15) Shen, T.; Penumatcha, A. V.; Appenzeller, J., Strain Engineering for Transition Metal Dichalcogenides Based Field Effect Transistors. *ACS Nano* **2016**, *10* (4), 4712-4718.
- (16) Castellanos-Gomez, A.; Roldán, R.; Cappelluti, E.; Buscema, M.; Guinea, F.; van der Zant, H. S. J.; Steele, G. A., Local Strain Engineering in Atomically Thin MoS₂. *Nano Lett.* **2013**, *13* (11), 5361-5366.
- (17) Novoselov, K. S.; Geim, A. K.; Morozov, S. V.; Jiang, D.; Zhang, Y.; Dubonos, S. V.; Grigorieva, I. V.; Firsov, A. A., Electric Field Effect in Atomically Thin Carbon Films. *Science* **2004**, *306* (5696), 666.
- (18) Lee, C.-H., *et al.*, Atomically thin p-n junctions with van der Waals heterointerfaces. *Nat Nano* **2014**, *9* (9), 676-681.

- (19) Kang, K.; Lee, K.-H.; Han, Y.; Gao, H.; Xie, S.; Muller, D. A.; Park, J., Layer-by-layer assembly of two-dimensional materials into wafer-scale heterostructures. *Nature* **2017**, *advance online publication*.
- (20) Tao, P.; Guo, H.-H.; Yang, T.; Zhang, Z.-D., Stacking stability of MoS₂ bilayer: An ab initio study. *Chinese Physics B* **2014**, *23* (10), 106801.
- (21) He, J.; Hummer, K.; Franchini, C., Stacking effects on the electronic and optical properties of bilayer transition metal dichalcogenides MoS₂, MoSe₂, WS₂, and WSe₂. *Phys. Rev. B* **2014**, *89* (7), 075409-11.
- (22) Kushima, A.; Qian, X.; Zhao, P.; Zhang, S.; Li, J., Ripplings in van der Waals Layers. *Nano Lett.* **2015**, *15* (2), 1302-1308.
- (23) Shanshan, W.; Merce, P.; Harish, B.; Jamie, H. W., Substrate control for large area continuous films of monolayer MoS₂ by atmospheric pressure chemical vapor deposition. *Nanotechnology* **2016**, *27* (8), 085604.
- (24) Plimpton, S., Fast Parallel Algorithms for Short-Range Molecular-Dynamics. *Journal of Computational Physics* **1995**, *117* (1), 1-19.
- (25) Brenner, D. W.; Shenderova, O. A.; Harrison, J. A.; Stuart, S. J.; Ni, B.; Sinnott, S. B., A second-generation reactive empirical bond order (REBO) potential energy expression for hydrocarbons. *J. Phys.: Condens. Matter* **2002**, *14* (4), 783-802.
- (26) Liang, T.; Phillpot, S. R.; Sinnott, S. B., Parametrization of a reactive many-body potential for Mo-S systems. *Phys. Rev. B* **2009**, *79* (24), 245110-14.
- (27) Stewart, J. A.; Spearot, D. E., Atomistic simulations of nanoindentation on the basal plane of crystalline molybdenum disulfide (MoS₂). *Modell. Simul. Mater. Sci. Eng.* **2013**, *21* (4), 045003-15.
- (28) Grimme, S., Semiempirical GGA-type density functional constructed with a long-range dispersion correction. *J. Comput. Chem.* **2006**, *27* (15), 1787-1799.
- (29) Han, Y.; Li, M.-Y.; Jung, G.-S.; Marsalis, M. A.; Qin, Z.; Buehler, M. J.; Li, L.-J.; Muller, D. A., Sub-nanometre channels embedded in two-dimensional materials. *Nat. Mater.* **2017**.
- (30) Tao, P.; Guo, H.-H.; Yang, T.; Zhang, Z.-D., Stacking stability of MoS₂ bilayer: An ab initio study. *Chinese Physics B* **2014**, *23* (10), 106801-6.
- (31) Izrailev, S.; Stepaniants, S.; Isralewitz, B.; Kosztin, D.; Lu, H.; Molnar, F.; Wriggers, W.; Schulten, K., Steered Molecular Dynamics. In *Computational Molecular Dynamics: Challenges, Methods, Ideas: Proceedings of the 2nd International Symposium on Algorithms for Macromolecular Modelling, Berlin, May 21-24, 1997*, Deuffhard, P.; Hermans, J.; Leimkuhler, B.; Mark, A. E.; Reich, S.; Skeel, R. D., Eds. Springer Berlin Heidelberg: Berlin, Heidelberg, 1999; pp 39-65.
- (32) Jung, G. S.; Buehler, M. J., Multiscale Modeling in Muscular-Skeletal Systems. *Annu. Rev. Biomed. Eng.* **2017**, *19* (1).

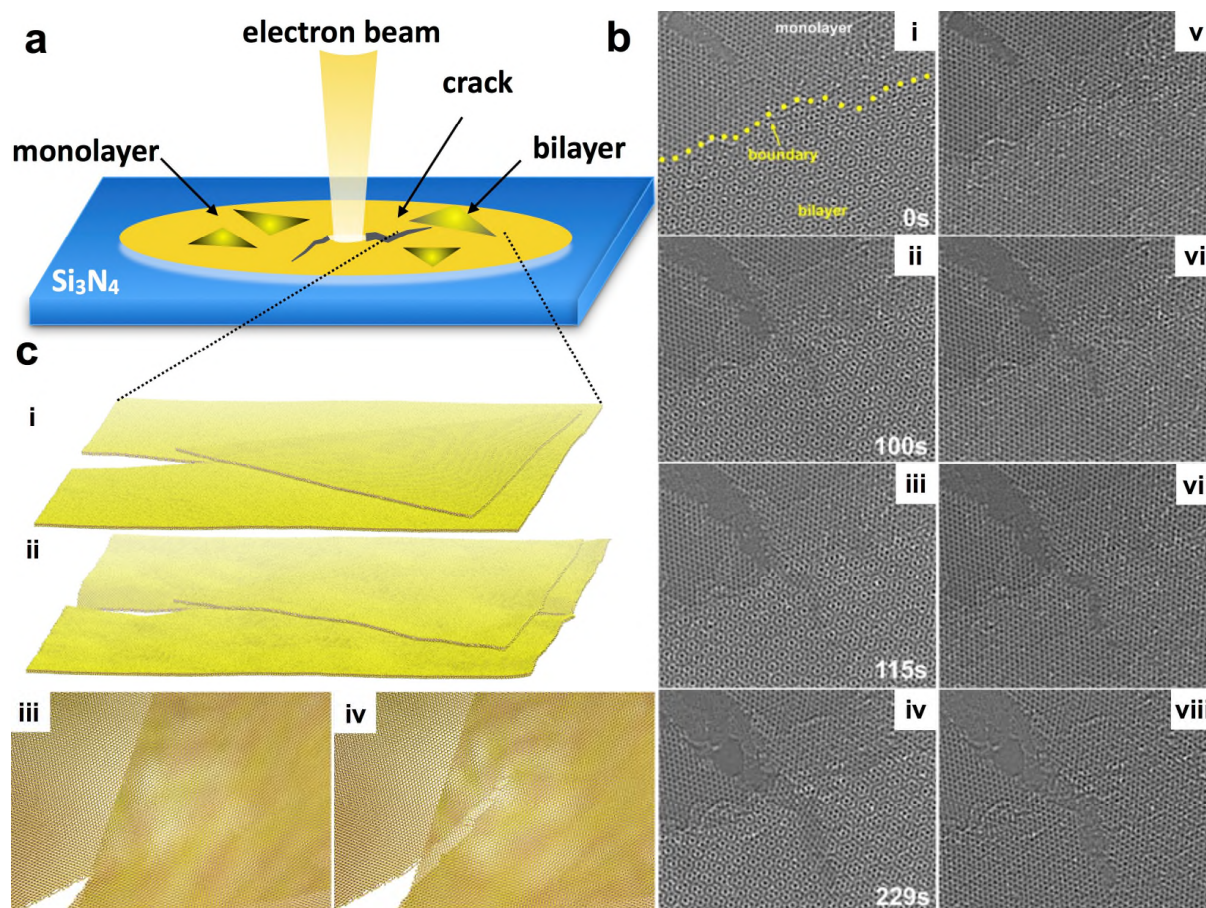


Figure 1. (a) Schematic illustration showing CVD grown mono- and bi-layer MoS₂ on Si₃N₄ TEM grid. The focused e-beam on the suspended layers generates a hole and cracks. Further (b) (A time series of AC-TEM images (i-iv) showing a crack going from the monolayer into the turbostratically-stacked bilayer region. The color of these AC-TEM images is inverted to give a higher visual contrast so that atoms are in white. The crack is restricted in one layer even in the bilayer region. (v-viii) A time series of reconstructed AC-TEM images after filtering out the uncracked layer. (c) The snapshots of MD simulation before (i, iii) and after (ii, iv) crack propagation into the triangular bilayer region. The crack is slightly defected as observed in AC-TEM images.

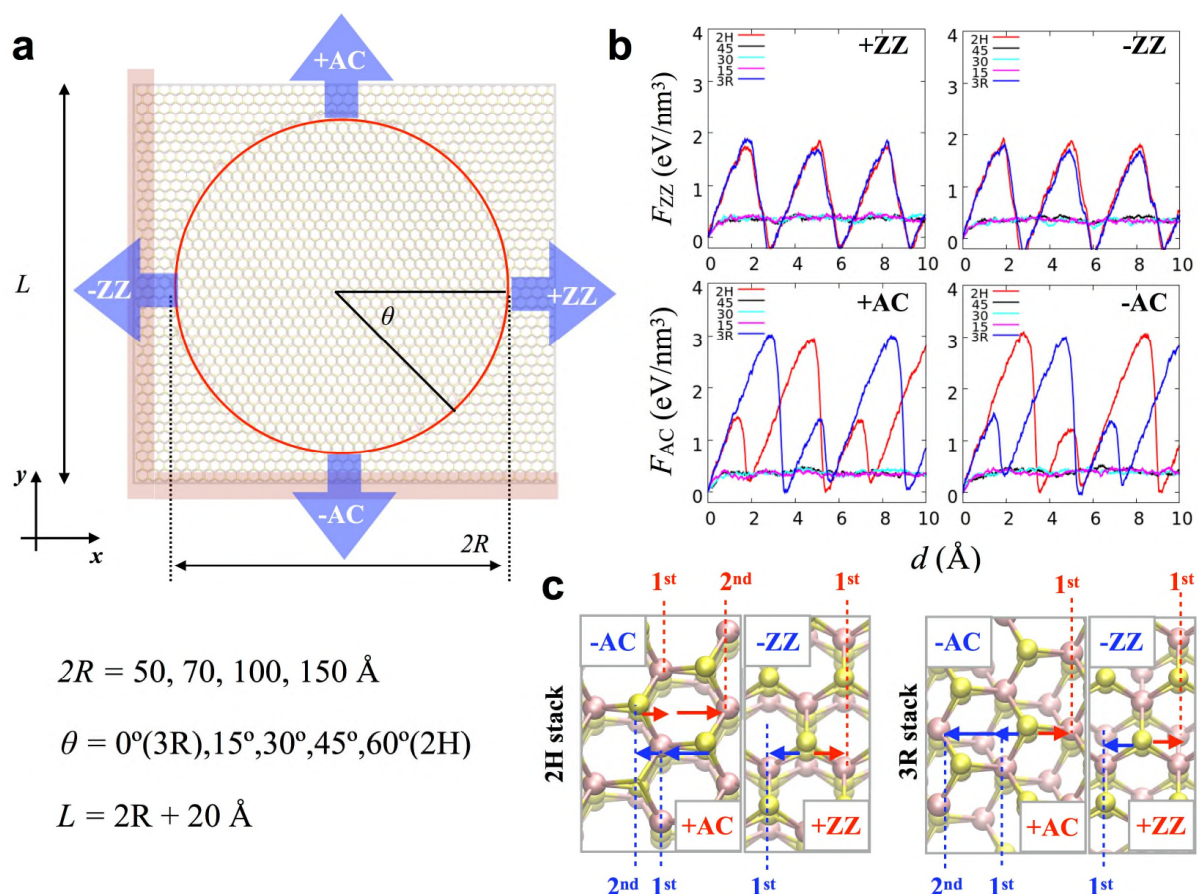


Figure 2. (a) Schematic description of MD simulations for interlayer frictional forces per area (eV/nm^3) with four different loading directions: positive and negative zigzag (+ZZ and -ZZ) and armchair directions (+AC and -AC). (b) The forces obtained from the system size of $2R = 15\text{nm}$ (c) The relative positions of sulfurs of top and bottom layers. Considering the small difference from the weak van der Waals interactions, the significant difference of friction forces is counterintuitive. The forces and directional dependency can be explained with the relative distance and position of sulfur atoms, suggesting the friction is originated from the geometrical interlocking. The detailed values for all samples are listed in the [Table S5 - S8](#).

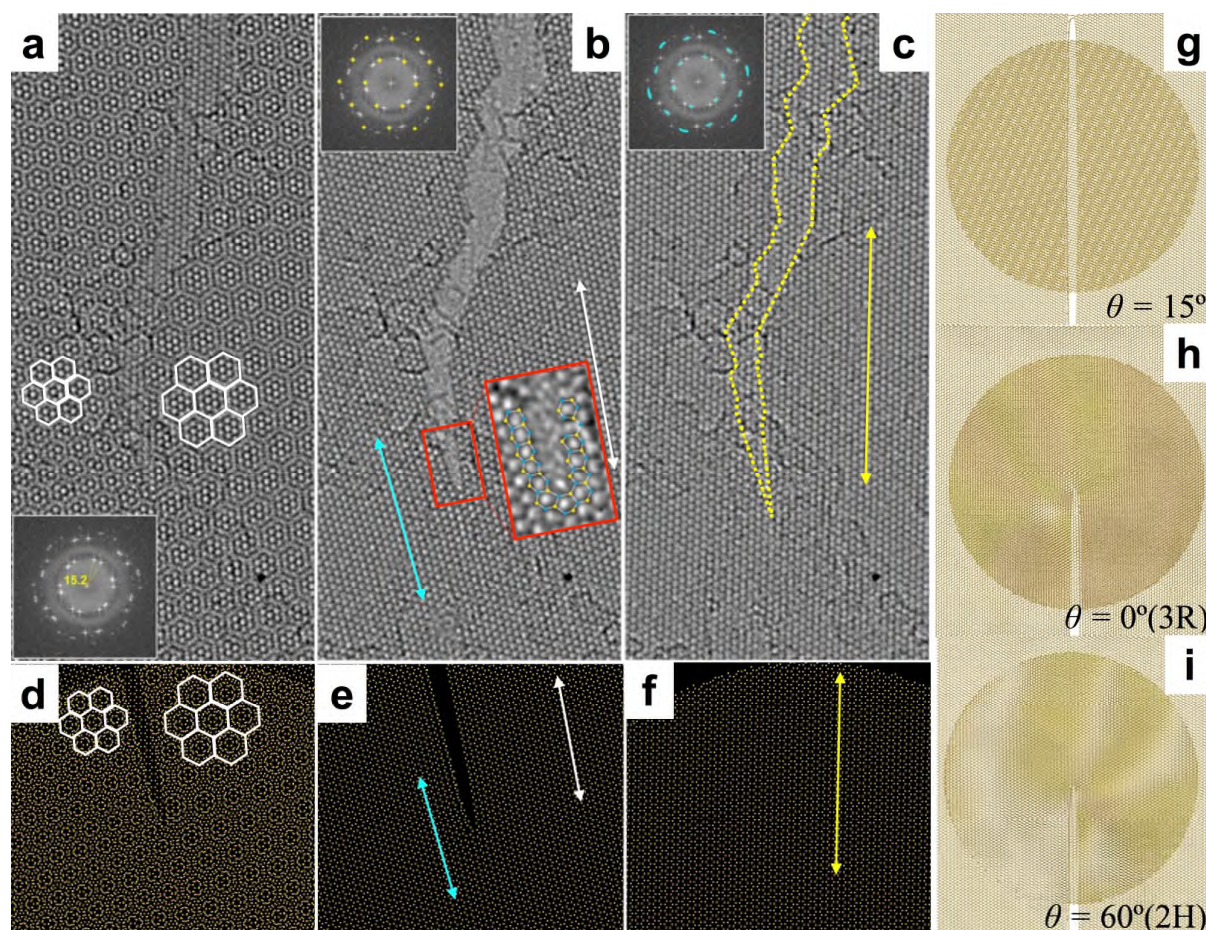


Figure 3. (a) AC-TEM image showing a crack propagating in one layer of a turbostratically assembled bilayer MoS₂. Inset shows the 2D FFT of the AC-TEM image, indicating the twist angle between two layers is around 15 degrees. (b) Reconstructed AC-TEM image after applying a mask to 2D FFT of panel a to remove the lattice contribution from the uncracked layer of MoS₂ (as shown the yellow dots of inset at the top left corner). It highlights the lattice configuration of the fractured layer. The crack tip region is zoomed-in with atomic models overlaid, which shows atomic sharpness. The blue and yellow spheres represent Mo and S atoms, respectively. (c) Reconstructed AC-TEM image of the uncracked layer after filtering out the lattice contribution from the fractured layer. The yellow outline indicates the region that has a crack on the other layer. There are no obvious structural changes in this region on the uncracked layer. (d) The MD simulation of crack propagation into finite bilayer region that turbostratically is stacked with 15 degrees. The white hexagons indicate the size of moiré patterns and the asymmetric sizes show good agreement with those in AC-TEM image in panel a. (e) Crack-tip image in the cracked region (f) image of the un-cracked finite layer region. The arrows indicate the zigzag lattice direction in both AC-TEM images and MD. (g-h) The MD results of crack propagation with different stacking, showing clear difference. 2H and 3R stack block the crack propagation while the other stacks allow the crack propagate through entire layers (Figure S4 and Supporting Movies 1 and 2).

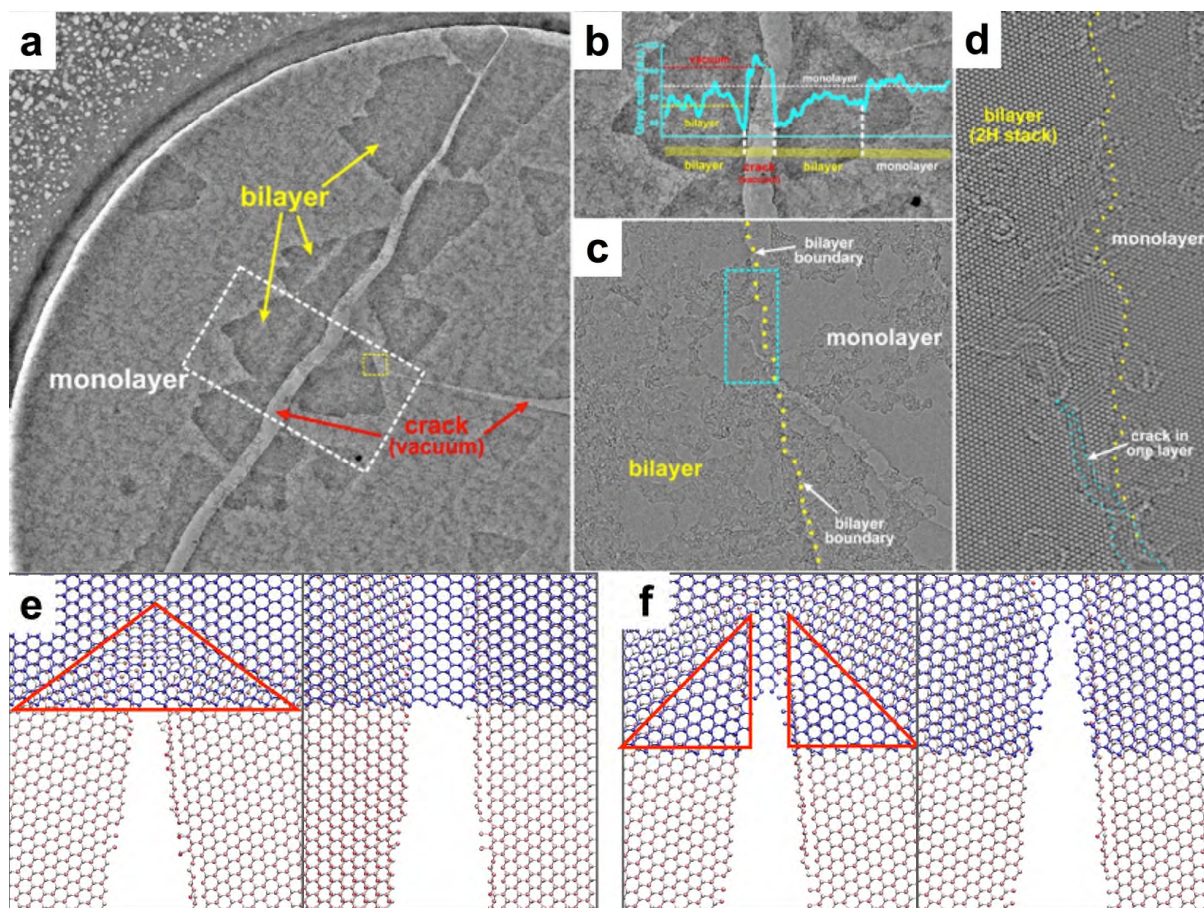


Figure 4. (a) Low-mag TEM image showing two cracks on a suspended MoS₂ region. Most areas of this suspended MoS₂ region is monolayer, with some small bilayer/multilayer islands distributed on it, as marked by yellow arrow. Two cracks can be observed. The red arrow on the left indicates one of them, and the other one is on the right. (b) Zoom-in TEM image of the region marked by the dashed white box on the left crack in panel a. Boxed intensity line profile along the yellow line is plotted, indicating different layer thickness in this measured region. It also confirms that both two layers fracture in this left crack, leaving vacuum in between. (c) Zoom-in TEM image of the region marked by the dashed yellow box at the tip region on the right crack of panel a. The crack goes from the monolayer MoS₂ into the bilayer region. The bilayer boundary is indicated by the yellow dotted line. The crack happens only in one layer in the bilayer region. (d) Zoom-in TEM image of the region in the cyan dashed box in panel c, confirming that the crack is restricted in one layer when it goes into the bilayer region. The bilayer boundary is marked by the yellow dashed line. The bilayer is in the 2H phase, having the most common AB stacking mode. In this stacking mode, the top and bottom MoS₂ layer are in the same lattice orientation. The S (Mo) atoms of each layer reside on the Mo (S) atoms on the other layer. Therefore, the bilayer region has the same hexagonal lattice pattern as that in the monolayer but having a darker contrast. Since the top and bottom layer are in the same lattice orientation, we cannot use the Fourier transform analysis to split the structure of each layer but can tell the layer thickness change by atomic column contrast. We use this method to tell the crack outline marked by the dashed cyan line. (e) Coherent fracture occurs when both layers move coherently during the crack propagation. The red triangle indicates the regions where the effective tensile stress locally occurs due to the high friction from 2H stack alignment. The top layer breaks after the crack pass through in the bottom layer. (f) The crack passes through in the bottom layer without breaking the other layer because effective tensile stress does not occur because of distorting lattice from 2H stack (See [Supporting Movies 3 and 4](#)).

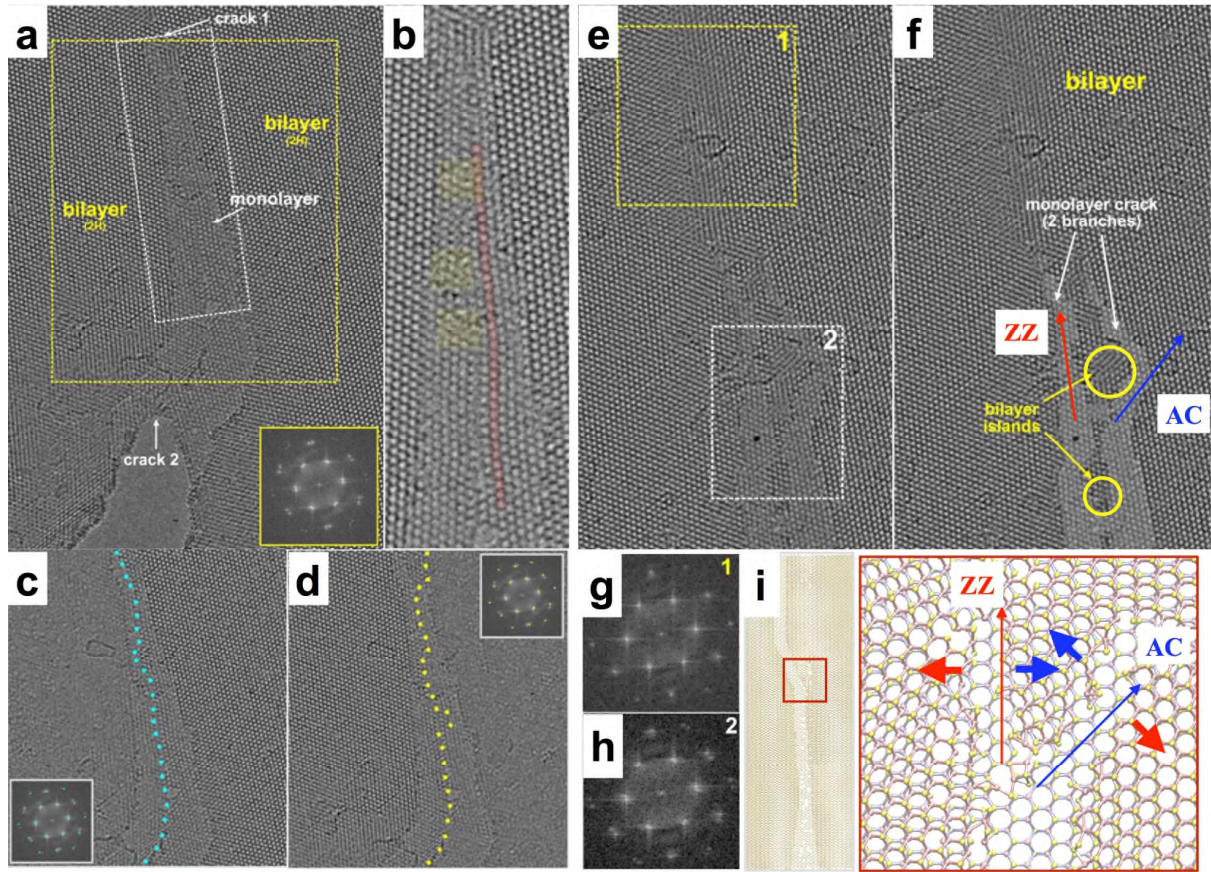


Figure 5. (a) AC-TEM image showing cracks in a 2H-stacked bilayer MoS₂ region. Cracks happen in both layers, with a crack in one layer going ahead of the other. Inset shows the 2D FFT of the region in the yellow dashed box. Two sets of FFT spots can be observed. There seems to be some special structure along the midcourt line of the uncracked monolayer region, as lattice shows distortion. (b) Zoom-in AC-TEM image of the region in the white dashed box in panel a, showing that the lattice in the monolayer region is deformed as indicated by the red region. In addition, there are many defects in this region, as marked by the half-transparent rectangles, which might be the reason of lattice distortion. (c) Reconstructed AC-TEM image after applying a mask to one set of the FFT spots, as indicated by the cyan spheres of inset. (d) Reconstructed AC-TEM image after applying a mask to the other set of the FFT spots, as indicated by the yellow spheres of inset. It can be seen that the boundary between the reserved and wiped regions is blurry, and this boundary is not exactly the same in panel b and c, which might be due to the close distance between these two sets of FFT spots. (e) AC-TEM image showing crack 1 in panel a branches off into two cracks, leaving some bilayer islands in between. Two cracks are highlighted by adding half-transparent white masks, as shown in panel (f). 2D FFT analysis are conducted in both the uncracked and cracked regions, marked by the yellow dashed and white dashed boxes in panel e. The FFT patterns 1 and 2 are shown in (g) and (h), respectively. The 2D FFT in the top uncracked region shows only one set of spots, while the FFT in the bottom cracked region shows two set of spots. (i) A crack branches in MD simulations because of defects in uncracked layer with constrained boundary conditions. The red arrows indicate the natural movement due to the external strain, while the blue arrows show the activation of high friction due to the relative configuration of other layers (See [Supporting Movies 5 and 6](#)).